Hindawi
Wireless Communications and Mobile Computing
Volume 2022, Article ID 6518066, 12 pages
https://doi.org/10.1155/2022/6518066

Research Article

Channel Measurement and Noise Estimation in FBMC/OQAM-Based IoT Networks

Jun Sun,[1,2] Xiaomin Mu,[1] and Dejin Kong[3]

[1]*School of Information Engineering, Zhengzhou University, Zhengzhou 450001, China*
[2]*School of Electronic and Information, Zhongyuan University of Technology, Zhengzhou 450007, China*
[3]*State Key Laboratory of New Textile Materials and Advanced Processing Technologies, The School of Electronic and Electrical Engineering, Wuhan Textile University, Wuhan 430200, China*

Correspondence should be addressed to Dejin Kong; djkou@wtu.edu.cn

Received 8 November 2021; Revised 14 December 2021; Accepted 17 December 2021; Published 10 January 2022

Academic Editor: Xingwang Li

Channel measurement plays an important role in the emerging 5G-enabled Internet of Things (IoT) networks, which reflects the channel quality and link reliability. In this paper, we address the channel measurement for link reliability evaluation in filter-bank multicarrier with offset quadrature amplitude modulation- (FBMC/OQAM-) based IoT network, which is considered as a promising technique for future wireless communications. However, resulting from the imaginary interference and the noise correlation among subcarriers in FBMC/OQAM, the existing frequency correlation method cannot be directly applied in the FBMC/OQAM-based IoT network. In this study, the concept of the block repetition is applied in FBMC/OQAM. It is demonstrated that the noises among subcarriers are independent by the block repetition and linear combination, instead of correlated. On this basis, the classical frequency correlation method can be applied to achieve the channel measurement. Then, we also propose an advanced frequency correlation method to improve the accuracy of the channel measurement, by assuming channel frequency responses to be quasi-invariant for several successive subcarriers. Simulations are conducted to validate the proposed schemes.

1. Introduction

The evaluation of the link reliability is required in the emerging 5G-enabled Internet of Things (IoT) networks, and based on the evaluation, the network performance can be enhanced by the power control or cell selection [1]. Therefore, the channel measurement plays a very important role in 5G-enabled IoT networks since it reflects the channel quality and link reliability. Generally speaking, the evaluation of the link reliability can be performed by measuring the received power of predefined reference signals [2]. In case of poor link, the base station can conduct the link switch, reducing the probability of network outage. In this study, we focus on the channel measurement for link reliability evaluation in filter-bank multicarrier with offset quadrature amplitude modulation- (FBMC/OQAM-) based IoT networks.

As one promising physical-layer technique for IoT networks, FBMC/OQAM exhibits the advantages of asynchronous transmissions owing to the low sidelobe of the spectrum [3, 4] and high spectral efficiency due to the avoidance of the cyclic prefix [5], compared with the classical orthogonal frequency division multiplexing (OFDM). However, due to the real-valued orthogonality, there is imaginary-valued interference among symbols in FBMC/OQAM, called as intrinsic imaginary interference. Resulting from intrinsic imaginary interference [6, 7], many existing algorithms for OFDM cannot be directly used in FBMC/OQAM, such as channel measurement. Since the long-term evolution (LTE) era, reference signal received power (RSRP) has been the key one of channel measurements by utilizing reference signals [8]. Currently, there have existed several algorithms for channel measurement and noise estimation. In [9], a discrete Fourier transform- (DFT-) based time-domain algorithm was presented by utilizing the property that energy of the time-domain channel is only concentrated on the taps corresponding to propagation paths. In

[10, 11], the authors proposed a frequency correlation algorithm by computing the correlation of the estimated frequency channel responses at adjacent subcarriers. Due to the low complexity and satisfactory performance, the classical frequency correlation method has been widely adopted for the channel measurement and noise estimation in various 3GPP proposals [10, 11]. However, these existing algorithms were proposed for OFDM-based networks. Due to the imaginary interference, channel measurement and noise estimation are more complicated in FBMC/OQAM systems. To the authors' knowledge, channel measurement has not been addressed for FBMC/OQAM-based IoT networks.

In this paper, we address channel measurement and estimation based on the FBMC/OQAM structure with block repetition. Firstly, we derive the noise distribution mathematically, which indicates that the noises at the receiver subcarriers are independent. On this basis, the classical frequency correlation method can be applied to achieve the channel measurement. Then, we also propose an advanced frequency correlation method to improve the accuracy of the channel measurement in FBMC/OQAM-based wireless networks, by assuming channel frequency responses to be quasi-invariant for several successive subcarriers. Numerical simulations have been conducted to validate the proposed schemes. The innovations are summarized as follows. The corresponding text is shown in the following:

(i) By using the block repetition, the noises at the receiver subcarriers are demonstrated to not be correlated, which is a key difference from the existing concept on noise distribution in FBMC/OQAM systems

(ii) Based on the mentioned-above features, the classical frequency correlation method can be employed in FBMC/OQAM to achieve the channel measurement

(iii) We propose an improved frequency correlation method to improve the accuracy of channel measurement."

2. Classical Frequency Correlation Method

The classical frequency correlation method has been proposed for the channel measurement in OFDM-based networks, which has been widely adopted in various 3GPP proposals [10, 11]. In this section, we firstly present the classical frequency correlation method and then specify the drawbacks when it is directly used for the channel measurement in FBMC/OQAM-based networks.

2.1. Channel Measurement in OFDM. For classical OFDM systems, the received signal at the receiver can be obtained [12]

$$y_m = H_m x_m + \eta_m, \tag{1}$$

where x_m is the transmitted symbol at the m-th subcarrier and H_m is the channel frequency response. The noise η_m is usually supposed to satisfy the Gaussian distribution with zero mean and variance σ^2 and be independent for different subcarriers in the classical OFDM systems.

Based on Equation (1), the frequency-domain channel estimation is obtained as

$$\widehat{H}_m = \frac{y_m}{x_m} = H_m + \frac{\eta_m}{x_m}. \tag{2}$$

Suppose that the transmitted symbol x_m has a unit power. The noise term η_m/x_m still satisfies the Gaussian distribution with variance σ^2 and is independent for different subcarriers, which can be denoted as ξ_m for simplicity.

Supposing M subcarriers used for the estimation and the channel frequency responses are quasi-invariant for adjacent subcarriers, then the channel measurement, i.e., RSRP, can be obtained by the following frequency correlation method [10, 11],

$$\mathrm{RSRP}_o = \left| \frac{1}{M-1} \sum_{m=0}^{M-2} \widehat{H}_m \widehat{H}_{m+1}^* \right|, \tag{3}$$

where $\widehat{H}_{m+1}^*$ is the conjugate of $\widehat{H}_{m+1}$. When $H_m = H_{m+1}$ and M goes to infinity, Equation (3) can be rewritten as

$$\begin{aligned} \mathrm{RSRP}_o &= \lim_{M\longrightarrow\infty} \left| \frac{1}{M-1} \sum_{m=0}^{M-2} (H_m + \xi_m)(H_{m+1} + \xi_{m+1})^* \right| \\ &= \lim_{M\longrightarrow\infty} \left| \frac{1}{M-1} \sum_{m=0}^{M-2} \left(H_m H_{m+1}^* + H_m \xi_{m+1}^* + \xi_m H_{m+1}^* + \xi_m \xi_{m+1}^* \right) \right|. \end{aligned} \tag{4}$$

Since the noise η_m is independent and identically distributed in the classical OFDM systems, the following equations hold:

$$\lim_{M\longrightarrow\infty} \frac{1}{M-1} \sum_{m=0}^{M-2} H_m \xi_{m+1}^* = 0, \tag{5}$$

$$\lim_{M\longrightarrow\infty} \frac{1}{M-1} \sum_{m=0}^{M-2} \xi_m H_{m+1}^* = 0, \tag{6}$$

$$\lim_{M\longrightarrow\infty} \frac{1}{M-1} \sum_{m=0}^{M-2} \xi_m \xi_{m+1}^* = 0. \tag{7}$$

Then, Equation (4) can be rewritten as

$$\begin{aligned} \mathrm{RSRP}_o &= \lim_{M\longrightarrow\infty} \left| \frac{1}{M-1} \sum_{m=0}^{M-2} (H_m + \xi_m)(H_{m+1} + \xi_{m+1})^* \right| \\ &= \lim_{M\longrightarrow\infty} \frac{1}{M-1} \sum_{m=0}^{M-2} H_m H_m^*, \end{aligned} \tag{8}$$

which represents the quality of the channel.

Subsequently, the estimation of noise variance in OFDM systems can be obtained by

$$\widehat{\varepsilon}_o = \frac{1}{M}\sum_{m=0}^{M-1} y_m y_m^* - \mathrm{RSRP}_o. \tag{9}$$

Note that $\widehat{\varepsilon}_o$ will be equal to σ^2 when M goes to infinity in the classical OFDM systems.

2.2. Channel Measurement in FBMC/OQAM. Different from the classical OFDM system, the transmitted signal of each FBMC/OQAM subcarrier gets through a pulse-shaping filter with low spectrum sidelobe, leading to the better spectral utilization and ability of asynchronous transmission. Figure 1 shows the system model of FBMC/OQAM with M subcarriers, in which $g[k]$ is the pulse-shaping filter, and $a_{m,n}$ is the transmitted real-valued symbol at the time-frequency position (m, n). Firstly, the real-valued symbols $a_{m,n}$ are multiplied by $e^{j\pi(m+n)/2}$, and get through the $M/2$ -point upsampling (corresponding to half symbol duration). Then, the obtained signal is filtered by $g[k]$, and the equivalent baseband transmitting signal of FBMC/OQAM can be written as [13, 14]

$$s[k] = \sum_{m=0}^{M-1}\sum_{n\in\mathbb{Z}} a_{m,n} g\left[k - n\frac{M}{2}\right] e^{j2\pi mk/M} e^{j\pi(m+n)/2}. \tag{10}$$

After passing a multipath channel, $r[k]$ is the received signal at the receiver. Then, the demodulation of the received signal can be approximately written as

$$\widehat{a}_{m,n} = \sum_{m=0}^{M-1}\sum_{n\in\mathbb{Z}} r[k] g\left[k - n\frac{M}{2}\right] e^{-j2\pi mk/M} e^{-j\pi(m+n)/2}. \tag{11}$$

Note that the maximum channel delay is usually much smaller than the symbol duration. And it is demonstrated in [13] that Equation (11) can be approximately written as [13]

$$\widehat{a}_{m,n} \approx H_{m,n}\left(a_{m,n} + ja^o_{m,n}\right) + \eta_{m,n}, \tag{12}$$

where $H_{m,n}$ is the channel frequency response at position (m, n). For the slowly time-varying channels, $H_{m,n} \approx H_{m,n+1}$. The term $ja^o_{m,n}$ is the imaginary interference to the symbol $a_{m,n}$, i.e.,

$$ja^o_{m,n} = \sum_{m_0\in\mathbb{Z}}\sum_{n_0\in\mathbb{Z}} a_{m_0,n_0}\zeta^{m_0,n_0}_{m,n}, (m_0, n_0) \neq (m, n), \tag{13}$$

where $\zeta^{m_0,n_0}_{m,n}$ is the imaginary interference factor in FBMC/OQAM and is defined as [13]

$$\zeta^{m_0,n_0}_{m,n} = \sum_{k=-\infty}^{\infty} g\left[k - n\frac{M}{2}\right] g\left[k - n_0\frac{M}{2}\right] e^{j2\pi k(m-m_0)/M} \times e^{j\pi(m+n-m_0-n_0)/2}. \tag{14}$$

Specifically when $(m, n) = (m_0, n_0)$, $\zeta^{m_0,n_0}_{m,n} = 1$. When $(m, n) \neq (m_0, n_0)$, $\zeta^{m_0,n_0}_{m,n}$ is imaginary-valued. It has been revealed that the value of $\zeta^{m_0,n_0}_{m,n}$ is close to zero when $|m - m_0| \geq 2$ or $|n - n_0| \geq 2$ [13], indicating that the imaginary interference to one symbol is mainly determined by its adjacent symbols. Besides, $\eta_{m,n}$ is the noise term in FBMC/OQAM systems and is written as

$$\eta_{m,n} = \sum_{k=-\infty}^{+\infty} \eta[k] g\left[k - n\frac{M}{2}\right] e^{-j2\pi mk/M} e^{-j\pi(m+n)/2}, \tag{15}$$

where $\eta[k]$ is the additional white Gaussian noise (AWGN) in wireless channels and is assumed to have a variance σ^2. It has been proven in [14] that, due to the real orthogonality condition of FBMC/OQAM, $\eta_{m,n}$ is of zero mean and has variance σ^2, while is related to η_{m_0,n_0} for $|m - m_0| \leq 1$ and $|n - n_0| \leq 1$, which is different from classical OFDM systems.

Motivated by the noise correlation mentioned above, pilots as shown in Figure 2 are required if the classical frequency correlation method in (3) is directly used for channel measurement and noise estimation in FBMC/OQAM systems. For the block of Figure 2, the symbols in the first column are set to zero to avoid interference from the previous block, and the symbols in the third column are set to zero to avoid interference from data. The nonzero pilots are in the second column, and it is noted that the pilots are designed to be scattered to ensure that the noise components for nonzero pilots are independent of each other. Assume that $a_{2p,1} = \pm 1$, and $a_{2p+1,1} = 0$ with $p = 0, 1, \cdots, M/2 - 1$. Then, Equation (12) can be rewritten as

$$\widehat{a}_{2p,1} = H_{2p,1} a_{2p,1} + \eta_{2p,1}. \tag{16}$$

By the frequency correlation method, the channel measurement of FBMC/OQAM can be obtained as

$$\mathrm{RSRP}_f = \left| \frac{1}{M/2 - 1} \sum_{m=0}^{M/2-2} \frac{\widehat{a}_{2p,1}}{a_{2p,1}} \left(\frac{a\wedge_{2(p+1),1}}{a_{2(p+1),1}} \right)^* \right|. \tag{17}$$

Subsequently, the estimation of noise variance in FBMC/OQAM systems can be obtained by

$$\widehat{\varepsilon}_f = \frac{2}{M}\sum_{m=0}^{M/2-1} \widehat{a}_{2p,1}\widehat{a}^*_{2p,1} - RSRP_f. \tag{18}$$

As presented above, the classical frequency correlation method can be directly used for channel measurement and noise estimation in FBMC/OQAM systems. However, it is noted that the accuracy of channel measurement depends on the number of samples. For a fixed frequency band, all subcarriers in OFDM can be used for the channel measurement, while only half of the subcarriers in FBMC/OQAM can be used for the channel measurement. Therefore, there exists a loss of channel measurement accuracy when the classical frequency correlation method is directly used in FBMC/OQAM systems.

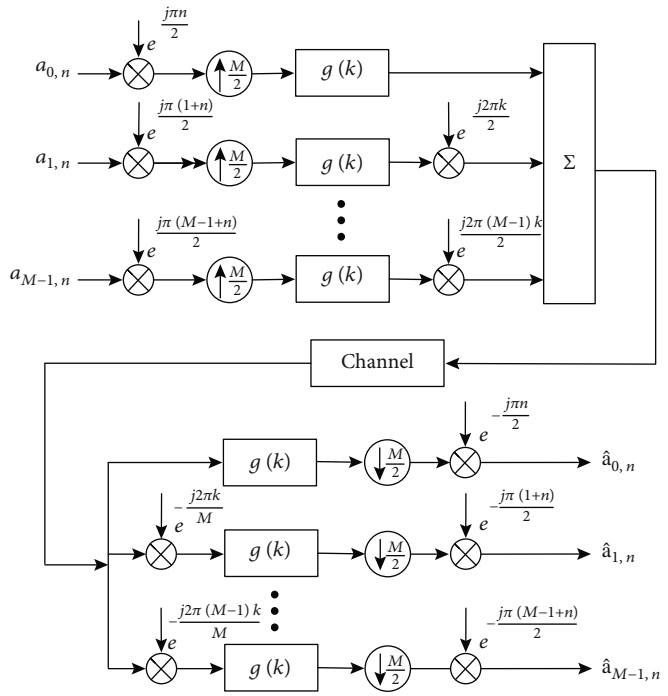

Figure 1: System model of FBMC/OQAM.

3. Proposed Scheme for Channel Measurement in FBMC/OQAM

In this section, we propose a novel scheme for channel measurement in FBMC/OQAM systems. Firstly, the imaginary interference factor is analyzed and it is noted that its amplitude is symmetric on the time-frequency position. Then, on the basis, a reversed-order repeated block is designed to remove the correlation among symbols so that all subcarriers can be used for the channel measurement in FBMC/OQAM systems, by the frequency correlation method, improving the RSRP accuracy.

3.1. Analysis of Imaginary Interference Factor. According to (14), the imaginary interference factor is defined as

$$\zeta_{m,n}^{m_0,n_0} = \sum_{k=-\infty}^{\infty} g\left[k - n\frac{M}{2}\right] g\left[k - n_0\frac{M}{2}\right] e^{j2\pi k(m-m_0)/M} \times e^{j\pi(m+n-m_0-n_0)/2}, \tag{19}$$

which is the interference coefficient to the symbol a_{m_0,n_0} from the symbol $a_{m,n}$. It is easily seen that the value of $\zeta_{m,n}^{m_0,n_0}$ only depends on the filter $g[k]$ and the time-frequency position (m, n). Note that the pulse-shaping filter $g[k]$ in FBMC/OQAM is real-valued and symmetric [15, 16]. Due to the fact that $g[k]$ is real-valued and symmetric, it can be easily demonstrated that the following equations hold

$$\zeta_{m_0,n_0}^{m_0,n_0-1} = -\zeta_{m_0,n_0}^{m_0,n_0+1}, \tag{20}$$

$$\zeta_{m_0,n_0}^{m_0-1,n_0} = -\zeta_{m_0,n_0}^{m_0+1,n_0}, \tag{21}$$

Pilot			Data						
0	1	0	$a_{0,3}$	$a_{0,4}$	$a_{0,5}$	$a_{0,6}$	$a_{0,7}$	$a_{0,8}$	$a_{0,9}$
0	0	0	$a_{1,3}$	$a_{1,4}$	$a_{1,5}$	$a_{1,6}$	$a_{1,7}$	$a_{1,8}$	$a_{0,9}$
0	−1	0	$a_{2,3}$	$a_{2,4}$	$a_{2,5}$	$a_{2,6}$	$a_{2,7}$	$a_{2,8}$	$a_{0,9}$
0	0	0	$a_{3,3}$	$a_{3,4}$	$a_{3,5}$	$a_{3,6}$	$a_{3,7}$	$a_{3,8}$	$a_{0,9}$
0	1	0	$a_{4,3}$	$a_{4,4}$	$a_{4,5}$	$a_{4,6}$	$a_{4,7}$	$a_{4,8}$	$a_{0,9}$
0	0	0	$a_{5,3}$	$a_{5,4}$	$a_{5,5}$	$a_{5,6}$	$a_{5,7}$	$a_{5,8}$	$a_{0,9}$

Figure 2: Scattered pilot for channel measurement and noise estimation in FBMC/OQAM.

$$\zeta_{m_0,n_0}^{m_0-1,n_0-1} = \zeta_{m_0,n_0}^{m_0-1,n_0+1} = \zeta_{m_0,n_0}^{m_0+1,n_0-1} = \zeta_{m_0,n_0}^{m_0+1,n_0+1}. \tag{22}$$

Furthermore, let $\bar{k} = k - n(M/2)$; then, Equation (19) can be rewritten as

$$\begin{aligned}\zeta_{m,n}^{m_0,n_0} &= \sum_{\bar{k}=-\infty}^{\infty} g[\bar{k}] g\left[\bar{k} + n\frac{M}{2} - n_0\frac{M}{2}\right] \times e^{j2\pi\left(\bar{k}+n(M/2)\right)(m-m_0)/M} e^{j\pi(m+n-m_0-n_0)/2} \\ &= \sum_{\bar{k}=-\infty}^{\infty} g[\bar{k}] g\left[\bar{k} + n\frac{M}{2} - n_0\frac{M}{2}\right] \times e^{j2\pi\bar{k}(m-m_0)/M} e^{j\pi(m-m_0)n} e^{j\pi(m+n-m_0-n_0)/2}.\end{aligned} \tag{23}$$

According to Equation (23), for adjacent subcarriers, i.e., $m - m_0 = \pm 1$, sign of $\zeta_{m,n}^{m_0,n_0}$ is opposite for the odd index n and the even index n. When the isotropic orthogonal transform algorithm (IOTA) is used for pulse shaping in FBMC/OQAM systems [14], the values of $\zeta_{m,n}^{m_0,n_0}$ are depicted in Tables 1 and 2 for the odd index and the even index,

respectively. Note that, as mentioned above, the value of $\zeta_{m,n}^{m_0,n_0}$ is close to zero when $|m-m_0| \geq 2$ and $|n-n_0| \geq 2$ [13]; therefore, Tables 1 and 2 only show the values of $\zeta_{m,n}^{m_0,n_0}$ for $|m-m_0| \leq 1$ and $|n-n_0| \leq 1$.

3.2. Reversed-Order Repeated Block. In this subsection, a reversed-order repeated block is presented to eliminate the correlation among adjacent subcarrier, utilizing the properties in (20)–(22), Tables 1 and 3. Assume that $a_{m,n}$ with $m = 0, 1, \cdots, M-1, n = 0, 1, \cdots, N-1$ are the transmitted symbols in FBMC/OQAM. Then, these symbols are transmitted repeatedly in the next block, satisfying $a_{m,N+n} = a_{m,N-1-n}$ with $n = 0, 1, \cdots, N-1$, as shown in Figure 3 in which $M = 6$ and $N = 5$ are taken as an example. Note that the symbol interval between $a_{m,n}$ and $a_{m,n+1}$ is still half of a quadrature amplitude modulation (QAM) symbol, exactly as the symbol interval of normal FBMC/OQAM systems.

After the modulation at the FBMC/OQAM transmitter and demodulation at the FBMC/OQAM receiver, demodulations of original symbols can be obtained as

$$\widehat{a}_{m,n} = H_{m,n}\left(a_{m,n} + ja_{m,n}^{o}\right) + \eta_{m,n}, n = 0, 1, \cdots, N-1, \quad (24)$$

and demodulations of repeated symbols can be obtained as

$$\begin{aligned}\widehat{a}_{m,2N-1-n} &= H_{m,2N-1-n}\left(a_{m,2N-1-n} + ja_{m,2N-1-n}^{o}\right)\\ &= H_{m,n}\left(a_{m,n} + ja_{m,2N-1-n}^{o}\right) + \eta_{m,2N-1-n}, n = 0, 1, \cdots, N-1.\end{aligned} \quad (25)$$

According to (13), the terms $ja_{m,n}^{o}$ and $ja_{m,2N-1-n}^{o}$ can be, respectively, written as

$$ja_{m,n}^{o} = \sum_{n_0=n-1}^{n+1}\sum_{m_0=m-1}^{m+1} a_{m_0,n_0}\zeta_{m,n}^{m_0,n_0}, (m_0, n_0) \neq (m, n), \quad (26)$$

$$ja_{m,2N-1-n}^{o} = \sum_{n_0=2N-2-n}^{2N-n}\sum_{m_0=m-1}^{m+1} a_{m_0,n_0}\zeta_{m,2N-1-n}^{m_0,n_0}, (m_0, n_0) \neq (m, 2N-1-n), \quad (27)$$

where $n = 0, 1, \cdots, N-1$.

Then, utilizing the properties of $\zeta_{m,n}^{m_0,n_0}$ in (20)–(22), Tables 1 and 3, and considering $a_{m,N+n} = a_{m,N-1-n}$ with $n = 0, 1, \cdots, N-1$ as shown in Figure 3, it can be easily demonstrated that the following equation holds:

$$ja_{m,n}^{o} + ja_{m,2N-1-n}^{o} = 0. \quad (28)$$

On this basis, it can be obtained as

$$\frac{\widehat{a}_{m,n} + \widehat{a}_{m,2N-1-n}}{2} = H_{m,n}a_{m,n} + \frac{\eta_{m,n} + \eta_{m,2N-1-n}}{2}. \quad (29)$$

From Equation (29), it is easily realized that the imaginary interference in FBMC/OQAM is removed by the linear combination. Figure 4 depicts the diagram of the imaginary interference cancelation in FBMC/OQAM, and compared with the classical scheme, the key differences are the employment of repeated symbols at the transmitter and the operation of the linear combination at the receiver. At the transmitter, the employment of repeated symbols does not increase additional add operations and multiplication operations. At the receiver, the linear combination only requires add operations, instead of multiplication operations. As a result, the complexity of the proposed scheme is almost the same as the classical scheme.

Table 1: $\zeta_{m,n}^{m_0,n_0}$ with odd time index n.

	n_0-1	n_0	n_0+1
m_0-1	$0.2280j$	$0.4411j$	$0.2280j$
m_0	$0.4411j$	1	$-0.4411j$
m_0+1	$0.2280j$	$-0.4411j$	$0.2280j$

Table 2: Simulation parameters.

Modulation	4QAM
Sampling frequency (MHz)	9.14
Number of paths	6
Power profile (in dB)	-6, 0, -7, -22, -16, -20
Delay profile (μs)	-3, 0, 2, 4, 7, 11

3.3. Analysis of Noise Distribution. It is noteworthy that, although the intersymbol interference is removed in Equation (29), the classical frequency correlation method is still not applicable for the channel measurement in FBMC/OQAM if the noise in (29) is not independent. Note that the noises at the receive subcarriers are correlated in the classical FBMC/OQAM structure without symbol repetition [14], due to its only real-filed orthogonality condition.

In this subsection, the distribution of noise term $\eta_{m,n} + \eta_{m,2N-1-n}/2$ in (29) is analyzed, and it will be demonstrated theoretically that the noises $\eta_{m,n} + \eta_{m,2N-1-n}/2$ are independent for different m, which is a key difference from the existing concept of noise distribution in FBMC/OQAM systems.

According to Equation (15), $\eta_{m,n}$ and $\eta_{m,2N-1-n}$ can be, respectively, written as

$$\eta_{m,n} = \sum_{k=-\infty}^{+\infty}\eta[k]g\left[k - n\frac{M}{2}\right]e^{-j2\pi mk/M}e^{-j\pi(m+n)/2}, \quad (30)$$

$$\eta_{m,2N-1-n} = \sum_{k=-\infty}^{+\infty}\eta[k]g\left[k - (2N-1-n)\frac{M}{2}\right]e^{-j2\pi mk/M} \times e^{-j\pi(m+2N-1-n)/2}, \quad (31)$$

where $n = 0, 1, \cdots, N-1$. Note that $\eta[k]$ is the AWGN noise in wireless channels and satisfies

$$\mathbb{E}\{\eta[k]\} = 0, \quad (32)$$

$$\mathrm{Var}\{\eta[k]\} = \sigma^2, \quad (33)$$

$$\mathrm{Cov}\{\eta[k], \eta[k_0]\} = 0, k \neq k_0, \quad (34)$$

Table 3: $\zeta_{m,n}^{m_0,n_0}$ with even time index n.

	n_0-1	n_0	n_0+1
m_0-1	-0.2280j	-0.4411j	-0.2280j
m_0	0.4411j	1	-0.4411j
m_0+1	-0.2280j	0.4411j	-0.2280j

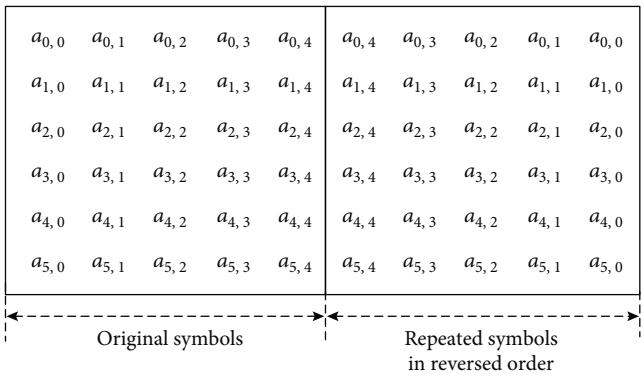

Figure 3: The reversed-order block for FBMC/OQAM.

where $\mathbb{E}\{\cdot\}$, $\mathrm{Var}\{\cdot\}$, and $\mathrm{Cov}\{\cdot\}$ are the operators of the expectation, variance, and covariance, respectively. As a result, the mean of $\eta_{m,n}$ is obtained as

$$\begin{aligned}\mathbb{E}\left[\eta_{m,n}\right] &= \mathbb{E}\left\{\sum_{k=-\infty}^{+\infty}\eta[k]g\left[k-n\frac{M}{2}\right]e^{-j2\pi mk/M}e^{-j\pi(m+n)/2}\right\}\\ &= \sum_{k=-\infty}^{+\infty}\mathbb{E}\{\eta[k]\}g\left[k-n\frac{M}{2}\right]e^{-j2\pi mk/M}e^{-j\pi(m+n)/2}=0.\end{aligned} \tag{35}$$

Note that Equation (35) holds for any m and n; hence, the mean of $\eta_{m,2N-1-n}$ is also zero.

Then, for the sake of simplicity, define

$$\chi_{m,n}=\frac{\eta_{m,n}+\eta_{m,2N-1-n}}{2}. \tag{36}$$

As mentioned above, $\eta_{m,n}$ and $\eta_{m,2N-1-n}$ satisfy the Gaussian distribution. Since $\chi_{m,n}$ is the linear combination of $\eta_{m,n}$ and $\eta_{m,2N-1-n}$, it can be realized that $\chi_{m,n}$ also satisfies the Gaussian distribution. The mean of $\chi_{m,n}$ can be obtained as

$$\mathbb{E}\left\{\chi_{m,n}\right\}=\mathbb{E}\left\{\frac{\eta_{m,n}}{2}\right\}+\mathbb{E}\left\{\frac{\eta_{m,2N-1-n}}{2}\right\}=0. \tag{37}$$

The variance of $\chi_{m,n}$ can be obtained as

$$\begin{aligned}\mathrm{Var}\left\{\chi_{m,n}\right\} &= \mathbb{E}\left\{\chi_{m,n}\chi_{m,n}^*\right\}-\mathbb{E}\left\{\chi_{m,n}\right\}\mathbb{E}\left\{\chi_{m,n}^*\right\}\\ &= \mathbb{E}\left\{\chi_{m,n}\chi_{m,n}^*\right\}=\frac{1}{4}\left[\mathbb{E}\left\{\eta_{m,n}\eta_{m,n}^*\right\}+\mathbb{E}\left\{\eta_{m,n}\eta_{m,2N-1-n}^*\right\}\right.\\ &\quad\left.+\mathbb{E}\left\{\eta_{m,2N-1-n}\eta_{m,n}^*\right\}+\mathbb{E}\left\{\eta_{m,2N-1-n}\eta_{m,2N-1-n}^*\right\}\right].\end{aligned} \tag{38}$$

Note that $\mathbb{E}\{\eta_{m,n}\eta_{m_0,n_0}^*\}$ can be written as

$$\begin{aligned}\mathbb{E}\left\{\eta_{m,n}\eta_{m_0,n_0}^*\right\} &= \mathbb{E}\left\{\left(\sum_{k=-\infty}^{+\infty}\eta[k]g\left[k-n\frac{M}{2}\right]e^{-j2\pi mk/M}e^{-j\pi(m+n)/2}\right)\right.\\ &\quad\left.\cdot\left(\sum_{k=-\infty}^{+\infty}\eta^*[k]g\left[k-n_0\frac{M}{2}\right]e^{j2\pi m_0k/M}e^{j\pi(m_0+n_0)/2}\right)\right\}\\ &= \mathbb{E}\left\{\sum_{k=-\infty}^{+\infty}\eta[k]\eta^*[k]g\left[k-n\frac{M}{2}\right]g\left[k-n_0\frac{M}{2}\right]\right.\\ &\quad\left.\times e^{-j2\pi(m-m_0)k/M}e^{-j\pi(m+n-m_0-n_0)/2}\right\}.\end{aligned} \tag{39}$$

According to the definition of the imaginary interference factor in Equation (14), we can rewrite (39) as

$$\mathbb{E}\left\{\eta_{m,n}\eta_{m_0,n_0}^*\right\}=\sigma^2\zeta_{m_0,n_0}^{m,n}. \tag{40}$$

Note that it has been realized in [13] that $\zeta_{m_0,n_0}^{m,n}$ is a pure imaginary value when $(m,n)\neq(m_0,n_0)$. And when $(m,n)=(m_0,n_0)$, the value of $\zeta_{m_0,n_0}^{m,n}$ is equal to 1, i.e.,

$$\zeta_{m,n}^{m,n}=1. \tag{41}$$

Furthermore, it has been revealed that the value of $\zeta_{m_0,n_0}^{m,n}$ is close to zero when $|m-m_0|\geq 2$ and $|n-n_0|\geq 2$ [13]. In addition, the term $\eta_{m,n}\eta_{m,2N-1-n}^*$ is the conjugate of $\eta_{m,2N-1-n}\eta_{m,n}^*$; hence, it can be obtained as $\mathbb{E}\{\eta_{m,n}\eta_{m,2N-1-n}^*\}+\mathbb{E}\{\eta_{m,2N-1-n}\eta_{m,n}^*\}=0$. Then, $\mathrm{Var}\{\chi_{m,n}\}$ can be obtained as

$$\begin{aligned}\mathrm{Var}\left\{\chi_{m,n}\right\} &= \frac{\mathbb{E}\left\{\eta_{m,n}\eta_{m,n}^*\right\}+\mathbb{E}\left\{\eta_{m,2N-1-n}\eta_{m,2N-1-n}^*\right\}}{4}\\ &= \frac{\sigma^2+\sigma^2}{4}=\frac{\sigma^2}{2}.\end{aligned} \tag{42}$$

Then, the covariance of $\chi_{m,n}$ and χ_{m_0,n_0} with $(m,n)\neq(m_0,n_0)$ is obtained.

$$\begin{aligned}\mathrm{Cov}\left\{\chi_{m,n},\chi_{m_0,n_0}\right\} &= \mathbb{E}\left\{\chi_{m,n}\chi_{m_0,n_0}^*\right\}-\mathbb{E}\left\{\chi_{m,n}\right\}\mathbb{E}\left\{\chi_{m_0,n_0}^*\right\}=\mathbb{E}\left\{\chi_{m,n}\chi_{m_0,n_0}^*\right\}\\ &= \frac{1}{4}\left[\mathbb{E}\left\{\eta_{m,n}\eta_{m_0,n_0}^*\right\}+\mathbb{E}\left\{\eta_{m,n}\eta_{m_0,2N-1-n_0}^*\right\}\right.\\ &\quad\left.+\mathbb{E}\left\{\eta_{m,2N-1-n}\eta_{m_0,n_0}^*\right\}+\mathbb{E}\left\{\eta_{m,2N-1-n}\eta_{m_0,2N-1-n_0}^*\right\}\right].\end{aligned} \tag{43}$$

Substituting Equations (39) and (40) into (43), it can be obtained as

$$\mathrm{Cov}\left\{\chi_{m,n},\chi_{m_0,n_0}\right\}=\frac{1}{4}\left[\sigma^2\zeta_{m_0,n_0}^{m,n}+\sigma^2\zeta_{m_0,2N-1-n_0}^{m,n}+\sigma^2\zeta_{m_0,n_0}^{m,2N-1-n}+\sigma^2\zeta_{m_0,2N-1-n_0}^{m,2N-1-n}\right]. \tag{44}$$

Note that, according to the definition of $\zeta_{m_0,n_0}^{m,n}$ in (14), the value of $\zeta_{m_0,n_0}^{m,n}$ only depends on the values of $(m-m_0)$ and $(n-n_0)$, instead of individual m, m_0, n, or n_0. Based

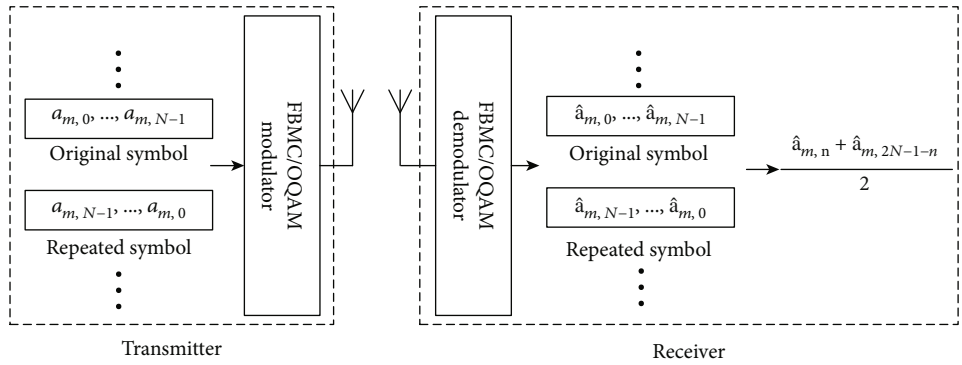

Figure 4: The scheme of the imaginary interference cancelation in FBMC/OQAM.

on the properties in (20)–(22), Tables 1 and 3, it can be obtained as

$$\mathrm{Cov}\left\{\chi_{m,n}, \chi_{m_0,n_0}\right\} = 0. \tag{45}$$

Therefore, it can be concluded that by the linear combination on the reversed-order block in Figure 3, the noise for the demodulated symbol is independent to each other. Note that it has been pointed out in [14] that the noise is correlated to that of its adjacent symbols in normal FBMC/OQAM without the reversed-order block.

Above all, Equation (29) in FBMC/OQAM will be equivalent to that of OFDM systems as Equation (2). Then, the classical frequency correlation method can be directly employed for channel measurement and noise estimation in FBMC/OQAM systems.

4. Proposed Channel Measurement in FBMC/OQAM

In this section, the channel measurement in FBMC/OQAM is presented based on the signal model as Equation (29), by using the classical frequency correlation method. Then, an improved frequency correlation method is proposed to improve the channel measurement accuracy.

4.1. Channel Measurement Using Classical Frequency Correlation. Figure 5 shows the proposed pilot design for channel measurement in FBMC/OQAM, in which $a_{m,0}$ with $m = 0, 1, \cdots, M-1$ are the pilots and $a_{m,n}$ with $n = 1, 2, \cdots, N-1$ are the data symbols. Note that all symbols in Figure 5 are complex-valued because the imaginary interferences among them can be eliminated completely by the linear combination in (29). As a consequence, compared with Figure 2, a lower pilot overhead is achieved in Figure 5.

According to (29), it can be obtained as

$$\frac{\widehat{a}_{m,0} + \widehat{a}_{m,2N-1}}{2a_{m,0}} = H_{m,0} + \frac{\eta_{m,0} + \eta_{m,2N-1}}{2a_{m,0}}. \tag{46}$$

For simplicity, denote $\widehat{a}_{m,0} + \widehat{a}_{m,2N-1}/2a_{m,0}$ as $\phi_{m,0}$, and denote $\eta_{m,0} + \eta_{m,2N-1}/2a_{m,0}$ as $\xi_{m,0}$. Then, (46) can be rewritten as

$$\phi_{m,0} = H_{m,0} + \xi_{m,0}, m = 0, 1, \cdots, M-1. \tag{47}$$

Note that, as analyzed in Section 3.2, the noise term $\xi_{m,0}$ satisfies independent identical distribution and its variance is $\sigma^2/2$ when pilots $a_{m,0}$ have the unit transmitting power.

Afterwards, the classical frequency correlation method can be directly used to obtain RSRP in FBMC/OQAM systems,

$$\mathrm{RSRP}_p = \left| \frac{1}{M-1} \sum_{m=0}^{M-2} \phi_{m,0} \phi_{m+1,0}^{*} \right|. \tag{48}$$

Subsequently, the estimation of noise variance can be obtained by

$$\widehat{\varepsilon}_p = 2\left(\frac{1}{M} \sum_{m=0}^{M-1} \phi_{m,0} \phi_{m,0}^{*} - \mathrm{RSRP}_p \right). \tag{49}$$

Different from Figure 2 in which only half of subcarriers are valid, all subcarriers are used for the channel measurement in Figure 5, indicating the improvement of accuracy in theory.

4.2. Improved Frequency Correlation Method. In this subsection, we propose an improved frequency correlation method to further improve the accuracy of channel measurement in FBMC/OQAM systems, by assuming the channel frequency responses quasi-invariant for several successive subcarriers. Subsequently, we give the theoretical analysis to show its superiority for the accuracy of channel measurement.

The frequency correlation method utilizes the properties of quasi-invariant channels for adjacent subcarrier and independent distribution of noises. It is realized that, by the linear combination on the reversed-order block, the noises in (47) are independent for different subcarrier in FBMC/OQAM systems. By assuming the channels to be quasi-invariant for several successive subcarriers, more samples can be used to achieve the channel measurement by the statistical methods. Different from the conventional frequency correlation method, the correlation operations are performed on the several successive subcarriers in the improved frequency correlation method, instead of only two subcarriers, as shown in Figure 6. Hence, the improved frequency

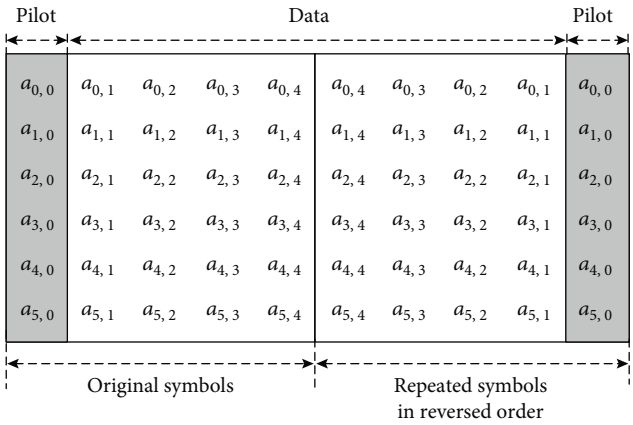

Figure 5: Proposed pilot design for channel measurement in FBMC/OQAM.

correlation method can be expressed as

$$\mathrm{RSRP}_i = \left| \frac{1}{N_c} \sum_{l=1}^{N_r-1} \sum_{m=0}^{M-l-1} \phi_{m,0} \phi_{m+l,0}^{*} \right|, \tag{50}$$

where N_r is the number of subcarriers whose channel frequency responses are quasi-invariant. N_c is the number of sum terms in (50), i.e.,

$$N_c = (M-1) + (M-2) + \cdots + (M-N_r+1) = \frac{(2M-N_r)(N_r-1)}{2}. \tag{51}$$

Subsequently, the estimation of noise variance can be obtained by

$$\widehat{\varepsilon}_i = 2\left(\frac{1}{M} \sum_{m=0}^{M-1} \phi_{m,0} \phi_{m,0}^{*} - \mathrm{RSRP}_i \right). \tag{52}$$

In theory, when the subcarrier number M goes to infinity, the channel measurement is accurate by the statistical method. However, M is limited in practice, leading to an interference. To evaluate the accuracy of the improved frequency correlation method, the variance of the residual interference is analyzed, in which the AWGN channel is assumed for simplicity. According to (50), the residual interference term can be easily written as

$$\Theta_i = \frac{1}{N_c} \sum_{l=1}^{N_r-1} \sum_{m=0}^{M-l-1} \left(\xi_{m,0} + \xi_{m+l,0}^{*} + \xi_{m,0} \xi_{m+l,0}^{*} \right). \tag{53}$$

Note that, for the classical frequency correlation method in (48), the residual interference term is

$$\Theta_p = \frac{1}{M-1} \sum_{m=0}^{M-2} \left(\xi_{m,0} + \xi_{m+1,0}^{*} + \xi_{m,0} \xi_{m+1,0}^{*} \right). \tag{54}$$

Since the noise term $\xi_{m,0}$ satisfies independent identical distribution, it is easily demonstrated that the expectations of Θ_p and Θ_i are equal to zero, i.e., $E[\Theta_i] = E[\Theta_p] = 0$. Then, the variances of Θ_p and Θ_i can be obtained as

$$\mathrm{Var}\left[\Theta_p\right] = \mathrm{E}\left[\Theta_p \Theta_p^{*}\right] - \mathrm{E}\left[\Theta_p\right] E\left[\Theta_p^{*}\right] = \frac{2\sigma^2 + \sigma^4}{2(M-1)}, \tag{55}$$

$$\mathrm{Var}[\Theta_i] = \mathrm{E}[\Theta_i \Theta_i^{*}] - \mathrm{E}[\Theta_i]\mathrm{E}[\Theta_i^{*}] = \frac{12(M-N_r+1) + 4(N_r-2)(2N_r-3)}{3(2M-N_r)^2(N_r-1)} \sigma^2 + \frac{1}{(2M-N_r)(N_r-1)} \sigma^4. \tag{56}$$

From Equations (55) and (56), when $N_r = 2$, it can be obtained as $\mathrm{Var}[\Theta_i] = \mathrm{Var}[\Theta_p]$ and the proposed frequency correlation method is equivalent to the classical frequency correlation method. When $N_r > 2$, $\mathrm{Var}[\Theta_i]$ will be smaller than $\mathrm{Var}[\Theta_p]$, and the proposed frequency correlation method can achieve better RSRP measurement performance than the conventional frequency correlation method. Especially when $M \gg N_r > 2$, the variance of Θ_i can be rewritten as

$$\begin{aligned} \mathrm{Var}[\Theta_i] &\approx \lim_{M/N_r \longrightarrow \infty} \left(\frac{12(M-N_r+1)}{3(2M-N_r)^2(N_r-1)} \sigma^2 + \frac{1}{(2M-N_r)(N_r-1)} \sigma^4 \right) \\ &= \lim_{M/N_r \longrightarrow \infty} \frac{4(M-N_r+1)\sigma^2 + (2M-N_r)\sigma^4}{(2M-N_r)^2(N_r-1)} \\ &= \lim_{M/N_r \longrightarrow \infty} \frac{4\sigma^2 + 2\sigma^4}{(4M-4N_r)(N_r-1)} = \lim_{M/N_r \longrightarrow \infty} \frac{2\sigma^2 + \sigma^4}{2(M-1)(N_r-1)} \\ &= \frac{1}{N_r-1} \lim_{M/N_r \longrightarrow \infty} \frac{2\sigma^2 + \sigma^4}{2(M-1)}. \end{aligned} \tag{57}$$

According to (55), we have

$$\mathrm{Var}[\Theta_i] = \frac{1}{N_r-1} \mathrm{Var}\left[\Theta_p\right], M \gg N_r > 2. \tag{58}$$

From Equation (58), the variance of Θ_i is approximately $1/N_r - 1$ of that of Θ_p when M/N_r goes to infinity, which indicates that the proposed frequency correlation method with M pilots can achieve similar accuracy of the classical frequency correlation method with $(N_r - 1)M$ pilots.

5. Simulation Results

In this section, numerical simulations are given to validate the proposed schemes. In our simulations, we consider an FBMC/OQAM system with 2048 subcarriers, in which the IOTA function is taken as the pulse-shaping filter [15]. Note that only a partial frequency band, i.e., 180 subcarriers is assigned for one user to achieve channel measurement and noise estimation. In addition, the detailed parameters for the multipath channel are listed as Table 3 [13].

Figure 7 shows the BER of FBMC/OQAM with the proposed repeated block under the AWGN channel, and for

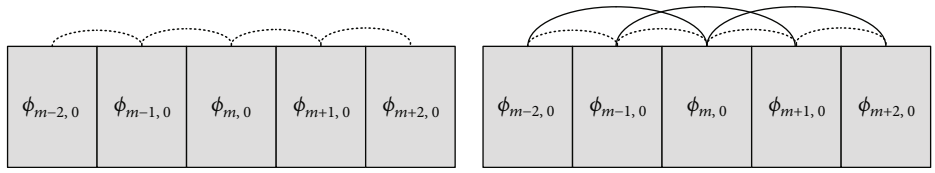

(a) Classical frequency correlation method (b) Proposed frequency correlation method

Figure 6: Proposed frequency correlation method.

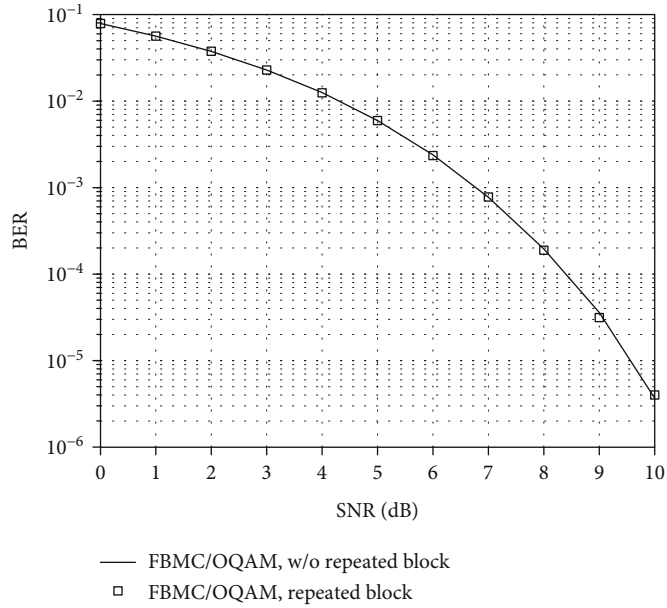

Figure 7: BER comparison in FBMC/OQAM, with or without repeated block.

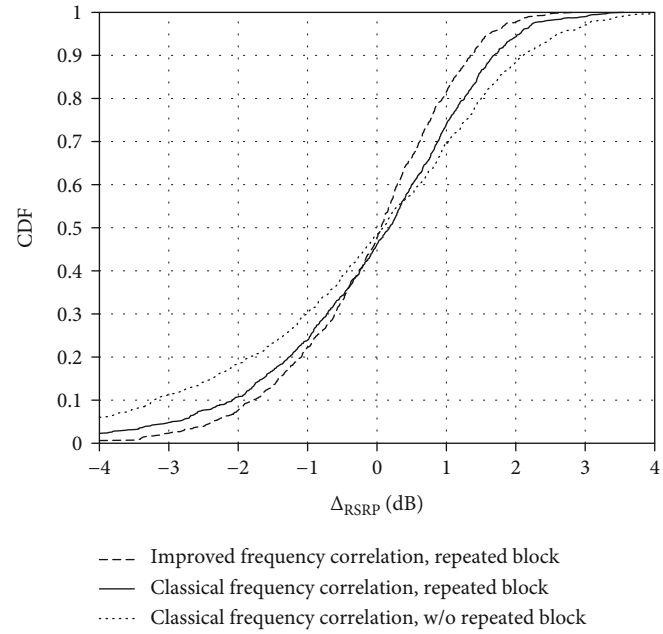

Figure 8: CDF of the proposed schemes under the AWGN channel, SNR = −6 dB.

comparison, the performance of FBMC/OQAM without the repeated block is also given. From the results, FBMC/OQAM with the proposed repeated block achieves the same BER performance as the FBMC/OQAM without repeated block, validating the effectiveness of the proposed scheme. As mentioned above, the imaginary interferences among

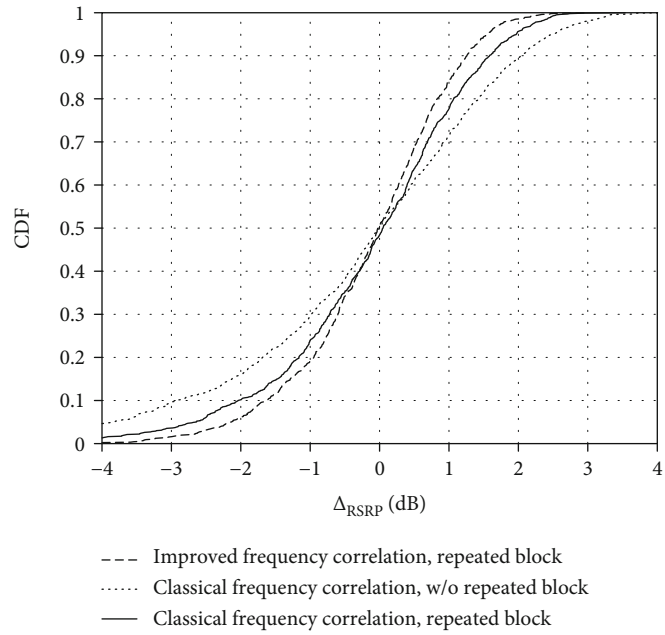

Figure 9: CDF of the proposed schemes under the multipath channel, SNR = −6 dB.

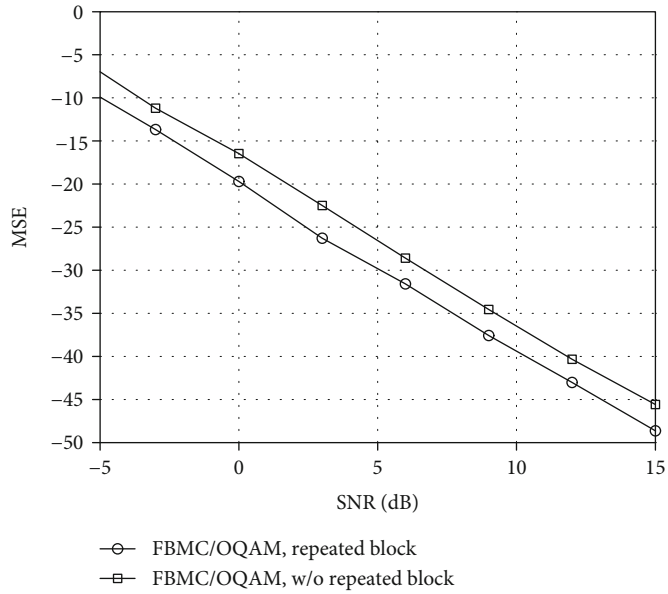

Figure 10: MSE of noise estimation in the proposed schemes under the AWGN channel.

symbols can be eliminated completely by the linear combination in (46); hence, complex-valued symbols can be directly transmitted if the reversed-order repeated block (Figure 5) is adopted. Note that the symbol interval is always $T/2$ in FBMC/OQAM. Therefore, FBMC/OQAM with the proposed repeated block can transmit $M \times N$ complex-valued symbols during the time $2N \times T/2 = NT$, while FBMC/OQAM without the repeated block can transmit $M \times 2N$ real-valued symbols during the time $2N \times T/2 = NT$. Therefore, the data rate is maintained in the proposed scheme. In addition, compared with FBMC/OQAM without repeated block, only the operation of the linear combination is required in FBMC/OQAM with repeated block; hence, the increase of complexity is negligible.

Figures 8 and 9 depict the cumulative distribution function (CDF) to evaluate the accuracy of channel measurement in FBMC/OQAM systems, in which the value Δ_{RSRP} represents the offset between the estimated RSRP and the ideal RSRP [17], i.e.,

$$\Delta_{RSRP} = 10 \log \left(RSRP_p\right) - 10 \log \left(RSRP_{ideal}\right). \quad (59)$$

When Δ_{RSRP} is closer to 0, the RSRP measurement is

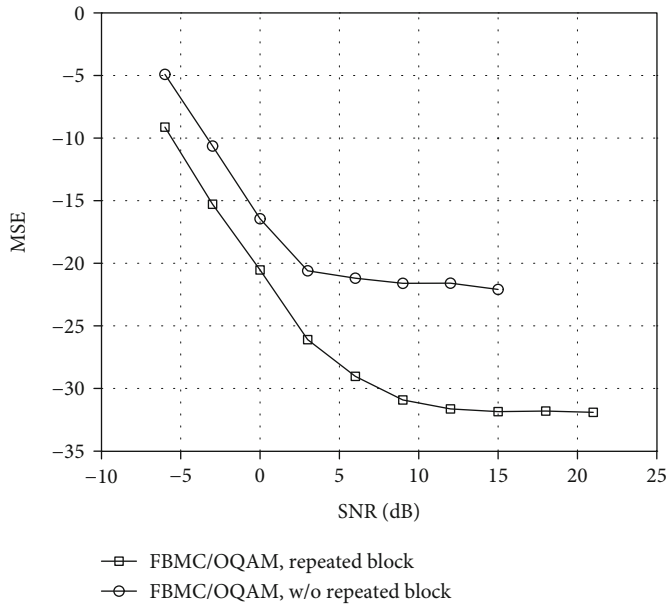

Figure 11: MSE of noise estimation in the proposed schemes under the multipath channel.

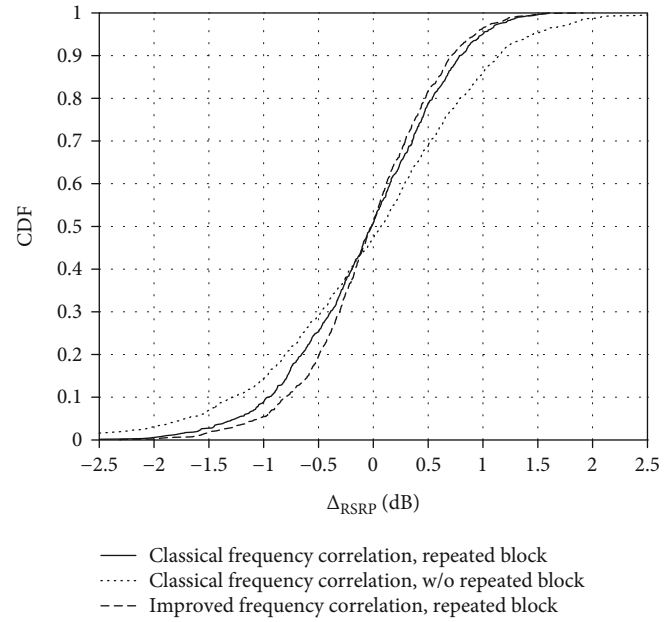

Figure 12: CDF of the proposed schemes under the LTE EPA channel, SNR = −6 dB.

more accurate. Otherwise, the accuracy of channel measurement is poor. In simulations, the AWGN channel is adopted in Figure 8 and the multipath channel is adopted in Figure 9, where SNR is set to be -6 dB [18]. From the simulation results, by the classical frequency correlation method, FBMC/OQAM with the proposed repeated block can achieve better RSRP accuracy than FBMC/OQAM without the repeated block. The reason is that, for the repeated block in Figure 5, all subcarriers can be utilized for the channel measurement since the imaginary interference can be completely removed by the linear combination in (46), while only half of subcarriers in Figure 2 can be utilized for the channel measurement. In addition, by the improved frequency correlation method, the RSRP accuracy can be further improved due to the increase of samples as mentioned in Section 4.2.

To evaluate the estimation accuracy of noise variance, Figures 10 and 11 show the mean square error (MSE) under the AWGN and multipath channels, respectively. From the simulation results, FBMC/OQAM with the proposed repeated block can achieve better estimation accuracy than FBMC/OQAM without the repeated block, due to the fact that all subcarriers are utilized for estimation in the proposed scheme. Especially, compared with Figure 10, there

exists the performance floor under the multipath channel in Figure 11. The reason is that the essence of the frequency correlation method is the correlation of adjacent subchannels that are assumed identical. However, multipath channels are frequency-selective. Therefore, there exists a bit of interference in the frequency correlation method. Note that the performance floor is above 23 dB for the conventional scheme while it is below 30 dB for the proposed scheme, indicating the superiority of the proposed scheme.

For more adequate evaluation, extended pedestrian A (EPA) model is also used in simulations, and Figure 12 depicts the CDF of the proposed scheme under the EPA channel, where SNR is set to be -6 dB. From the simulation results, by the classical frequency correlation method, FBMC/OQAM with the proposed repeated block can achieve better RSRP accuracy than FBMC/OQAM without the repeated block. In addition, by the improved frequency correlation method, the RSRP accuracy can be further improved. The conclusion is consistent to Figures 8 and 9.

6. Conclusions

In this paper, we addressed the channel measurement for link reliability in the FBMC/OQAM-based IoT networks, in which the block repetition was adopted. Firstly, The noise distribution was derived mathematically, which indicated that the noises at the receiver subcarriers are independent. Then, it was shown that the classical frequency correlation method could be applied to achieve the channel measurement, based on the noncorrelation of noises at the receiver subcarriers. Subsequently, an advanced frequency correlation method was proposed to improve the accuracy of the channel measurement in FBMC/OQAM-based wireless networks. Numerical simulations showed that the accuracy of channel measurement could be significantly improved by the proposed schemes.

Data Availability

The data used to support the findings of this study are available from the corresponding author upon request.

Conflicts of Interest

The authors declare that there are no conflicts of interest regarding the publication of this paper.

Acknowledgments

This work was financially supported in part by the National Science Foundation of China with Grant number 62001333.

References

[1] S. Sesia, M. Baker, and I. Toufik, *LTE: The UMTS Long Term Evolution: From Theory to Practice*, Wiley Publishing, 2009.

[2] T. Zhou, C. Tao, S. Salous, L. Liu, and Z. Tan, "Implementation of an LTE-based channel measurement method for high-speed railway scenarios," *IEEE Transactions on Instrumentation and Measurement*, vol. 65, no. 1, pp. 25–36, 2016.

[3] D. Kong, J. Li, K. Luo, and T. Jiang, "Reducing pilot overhead: channel estimation with symbol repetition in MIMO-FBMC systems," *IEEE Transactions on Communications*, vol. 68, no. 12, pp. 7634–7646, 2020.

[4] H. Wang, L. Xu, Z. Yan, and T. A. Gulliver, "Low-Complexity MIMO-FBMC sparse channel parameter estimation for industrial big data communications," *IEEE Transactions on Industrial Informatics*, vol. 17, no. 5, pp. 3422–3430, 2021.

[5] R. Nissel, S. Schwarz, and M. Rupp, "Filter bank multicarrier modulation schemes for future mobile communications," *IEEE Journal on Selected Areas in Communications*, vol. 35, no. 8, pp. 1768–1782, 2017.

[6] D. Kong, X. Zheng, Y. Zhang, and T. Jiang, "Frame repetition: a solution to imaginary interference cancellation in FBMC/OQAM systems," *IEEE Transactions on Signal Processing*, vol. 68, pp. 1259–1273, 2020.

[7] D. Kong, X. Zheng, Y. Tian, T. Jiang, and Y. Zhang, *Alamouti Code Based on Block Repetition in FBMC/OQAM Systems*, Appear to Digital Communications and Networks, 2021.

[8] 3GPP, *Evolved Universal Terrestrial Radio Access (E-UTRA); Physical layer; Measurements*, 2011, http://www.3gpp.org/ftp/Specs/archive/36_series/36.214/36214-a30.zip.

[9] G. Huang, A. Nix, and S. Armour, "DFT-based channel estimation and noise variance estimation techniques for single-carrier FDMA," in *IEEE Vehicular Technology Conference*, pp. 1–5, Ottawa, Canada, 2010.

[10] 3GPP TSG RAN WG4 63, TDocs R4-63AH-0145, *Further considerations for the feasibility research of CSI-RS based RSRP measurement*, Samsung, 2012.

[11] 3GPP TSG RAN WG4 63AH, TDocs R4-63AH-0084, *Further link level performance analysis of CSI-RS based RSRP measurements*, Intel Corporation, 2012.

[12] D. Kong, X.-G. Xia, P. Liu, and Q. Zhu, "MMSE channel estimation for two-port demodulation reference signals in new radio," *Science China Information Sciences*, vol. 64, pp. 169303:1–169303: 2, 2021.

[13] C. Lélé, J. P. Javaudin, R. Legouable, A. Skrzypczak, and P. Siohan, "Channel estimation methods for preamble-based OFDM/OQAM modulations," in *European Wireless Conference*, pp. 59–64, Paris, France, 2007.

[14] D. Kong, D. Qu, and T. Jiang, "Time domain channel estimation for OQAM-OFDM systems: algorithms and performance bounds," *IEEE Transactions on Signal Processing*, vol. 62, no. 2, pp. 322–330, 2014.

[15] A. Zafar, L. Zhang, P. Xiao, and M. A. Imran, "Spectrum efficient MIMO-FBMC system using filter output truncation," *IEEE Transactions on Vehicular Technology*, vol. 67, no. 3, pp. 2367–2381, 2018.

[16] J. Du and S. Signell, "Time frequency localization of pulse shaping filter in OFDM/OQAM systems," in *International Conference on Information, Communication and Signal Processing*, pp. 1–5, Singapore, 2007.

[17] 3GPP TSG RAN WG1 88, TDocs R1-1703097, *DL signals for mobility measurements in NR and mobility schemes*, Nokia, 2017.

[18] 3GPP TSG RAN WG1 87, TDocs R1-1612123, *DL RRM measurement over narrowband reference signals*, MediaTek, 2016.